Crystal structure of a eukaryotic (pea seedling) copper-containing amine oxidase at 2.2 Å resolution

Vinay Kumar[1†], David M Dooley[2*], Hans C Freeman[1*], J Mitchell Guss[3*], Ian Harvey[1‡], Michele A McGuirl[2], Matthew CJ Wilce[3] and Vilma M Zubak[1]

Background: Copper-containing amine oxidases catalyze the oxidative deamination of primary amines to aldehydes, in a reaction that requires free radicals. These enzymes are important in many biological processes, including cell differentiation and growth, wound healing, detoxification and signalling. The catalytic reaction requires a redox cofactor, topa quinone (TPQ), which is derived by post-translational modification of an invariant tyrosine residue. Both the biogenesis of the TPQ cofactor and the reaction catalyzed by the enzyme require the presence of a copper atom at the active site. The crystal structure of a prokaryotic copper amine oxidase from *E. coli* (ECAO) has recently been reported.

Results: The first structure of a eukaryotic (pea seedling) amine oxidase (PSAO) has been solved and refined at 2.2 Å resolution. The crystallographic phases were derived from a single phosphotungstic acid derivative. The positions of the tungsten atoms in the W_{12} clusters were obtained by molecular replacement using *E. coli* amine oxidase as a search model. The methodology avoided bias from the search model, and provides an essentially independent view of a eukaryotic amine oxidase. The PSAO molecule is a homodimer; each subunit has three domains. The active site of each subunit lies near an edge of the β-sandwich of the largest domain, but is not accessible from the solvent. The essential active-site copper atom is coordinated by three histidine side chains and two water molecules in an approximately square-pyramidal arrangement. All the atoms of the TPQ cofactor are unambiguously defined, the shortest distance to the copper atom being ~6 Å.

Conclusions: There is considerable structural homology between PSAO and ECAO. A combination of evidence from both structures indicates that the TPQ side chain is sufficiently flexible to permit the aromatic group to rotate about the Cβ–Cγ bond, and to move between bonding and non-bonding positions with respect to the Cu atom. Conformational flexibility is also required at the surface of the molecule to allow the substrates access to the active site, which is inaccessible to solvent, as expected for an enzyme that uses radical chemistry.

Addresses: [1]School of Chemistry, University of Sydney, NSW 2006, Australia, [2]Department of Chemistry and Biochemistry, Montana State University, Bozeman, MT 59717-0340, USA and [3]Department of Biochemistry, University of Sydney, NSW 2006, Australia.

Present addresses: [†]Solid State Physics Division, Bhaba Atomic Research Centre, Bombay-400085, India and [‡]School of Applied Sciences, De Montfort University, Leicester LE1 9BH, UK.

*Corresponding authors.
E-mail:
HCF, freemanh@chem.usyd.edu.au
DMD, uchdd@earth.oscs.montana.edu
JMG, m.guss@biochem.usyd.edu.au

Key words: amine oxidase, copper protein, crystal structure, topa quinone

Received: 16 May 1996
Revisions requested: 10 June 1996
Revisions received: 28 June 1996
Accepted: 1 July 1996

Structure 15 August 1996, 4:943–955

 ISSN 0969-2126

Introduction

Copper-containing amine oxidases catalyze the oxidative deamination of primary amines. The substrates are well known to be widely distributed and to participate in a large variety of biological processes, so that the enzymes are also likely to perform a diversity of functions. In eukaryotic organisms, the enzymes have been implicated in cell differentiation and growth, wound healing, detoxification and signalling [1–3]. The amine oxidation reaction is facilitated by a new type of cofactor, 2,4,5-trihydroxyphenylalanine quinone (topa quinone, TPQ), which is formed by post-translational modification of an invariant tyrosine residue. Although amine oxidases have been investigated intensively for over forty years, the first crystal structure — of an *E. coli* amine oxidase — was reported only recently [4].

There is evidence that the formation of the TPQ cofactor occurs via a novel self-processing mechanism in which a tyrosine residue is oxidized by protein-bound copper and oxygen [5,6]. Plausible reaction schemes have been summarised [7]. The modified tyrosine is part of a highly conserved sequence, Thr–X–X–Asn–Tyr–Asp/Glu. The copper atom is apparently required not only for the biogenesis of the functional quinone cofactor, but also for the catalytic oxidation of amines in the mature enzyme. To our knowledge, this is the first instance where the suitability of a metal for a particular biological setting may be

the result of two different, but perhaps related, selection criteria. The dual function of the copper atom has implications for the evolution of redox enzymes [8].

Although there may be some mechanistic variability, especially with regard to stereospecificity (see below), all copper-containing amine oxidases utilize a two-step, ping-pong type mechanism, illustrated in equations 1 and 2:

$$E+RCH_2NH_2 \rightarrow E\bullet RCH_2NH_2 \rightarrow E_{red}+RCHO \quad (1)$$

$$E_{red}+O_2 \rightarrow E+H_2O_2+NH_3 \quad (2)$$

An aminotransferase mechanism is operative (Fig. 1), involving proton abstraction from an imine intermediate to give a reduced, aminophenol form of the TPQ cofactor [1–3]. Kinetic isotope effects indicate that quantum mechanical tunnelling contributes significantly to the rate of proton abstraction [9,10]. Proton abstraction is stereospecific in some amine oxidases but not in others, and all the possible stereochemistries have been observed. Following aldehyde release, the reduced cofactor is reoxidized by molecular oxygen, most probably in two sequential 1-electron steps via a Cu(I)-semiquinone intermediate (Fig. 1) [11]. Intramolecular electron transfer to generate the Cu(I)-semiquinone has been shown to be kinetically feasible in amine oxidases from both eukaryotic (pea seedling) and prokaryotic (*Arthrobacter* P1) sources [12,13].

The crystal structure of a prokaryotic amine oxidase from *E. coli* (abbreviated as ECAO) has been reported recently [4]. The ECAO molecule was found to be a novel, mushroom-shaped dimer. Each of the two subunits has a large β-sandwich domain and three smaller α/β domains. The active site, which includes a Cu atom and a TPQ cofactor, is located in the large β-sandwich domain. Two remarkable β ribbon 'arms' from each subunit reach along the surface of the other subunit. One of the arms appears to be linked to the active site of the other subunit by a series of hydrogen bonds. Both an inactive form of ECAO (at 2.0 Å resolution) and an active form (at 2.4 Å resolution) were characterized. The only significant structural differences between the inactive and active forms of ECAO occur at the catalytic site.

Here we describe the first crystal structure of a eukaryotic amine oxidase, pea seedling amine oxidase (PSAO), and compare it with that of the prokaryotic *E. coli* enzyme. PSAO is an attractive candidate for X-ray crystallographic analysis for several reasons. A wealth of spectroscopic and mechanistic data for PSAO is waiting to be correlated with the molecular structure [1–3]. Most of the properties of PSAO are also expected to be typical of eukaryotic amine oxidases. Structural details that should be of interest include the locations of cysteine residues and glycosylation sites. The cysteine residues in PSAO are of interest

Figure 1

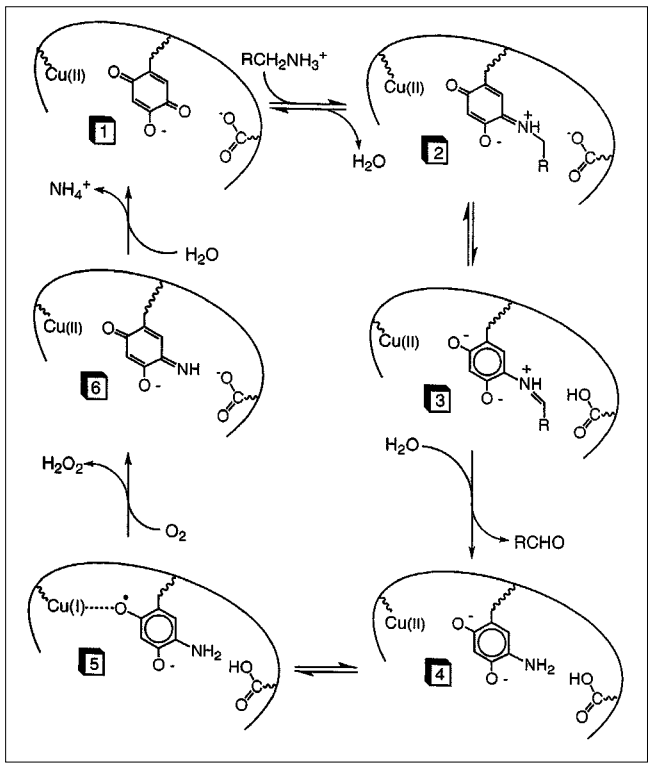

Proposed reaction scheme for the oxidation of amines by amine oxidases. The scheme is elaborated from that in [12] to show the proposed roles of the Cu atom, the cofactor topa quinone (TPQ), and the active-site base tentatively identified as Asp300 (represented by a carboxylate group). Schiff-base formation at C(5) of the TPQ (step 1→2) is followed by proton abstraction (step 2→3) and hydrolysis (step 3→4). The reduced, NH_2-substituted TPQ is reoxidized by dioxygen via a Cu(I)-semiquinone intermediate (steps 4→5→6), and TPQ is regenerated by hydrolysis (step 6→1). The scheme is of general applicability, with the exception that the stereospecificity of proton abstraction implied at step 2→3 operates differently (or not at all) in some amine oxidases.

because several of them are conserved among eukaryotic but not prokaryotic amine oxidases, and structural or functional roles for these residues have been proposed [14,15]. Identifying the number and locations of glycosylation sites in PSAO may be important as all eukaryotic amine oxidases are glycoproteins. On the other hand, PSAO has a distinctive substrate preference, being most active towards diamines, and in this respect differs from the mammalian plasma amine oxidases and the prokaryotic bacterial amine oxidases, whose preferred substrates are monoamines. Plant amine oxidases are also distinguished by having the highest turnover rates and the highest rates of re-oxidation of the reduced enzyme [1,3].

PSAO was crystallised in 1991 [16]. Only one heavy-atom reagent, phosphotungstic acid ($H_3PW_{12}O_{40}$), was found to yield an isomorphous derivative with appropriate diffraction properties. An electron-density map for this derivative

was calculated, using phases derived by molecular replacement with ECAO as the search model. The map enabled the positions of the 24 W atoms in the two $PW_{12}O_{40}$ clusters of the asymmetric unit to be located. The initial phases for the electron-density maps to which the protein structure was fitted were then derived from the contributions of the W atoms. The effect of this strategy was to eliminate bias from the molecular-replacement search model and to provide an essentially independent view of an amine oxidase structure.

Results and discussion

Molecular structure

The PSAO molecule is a dimer of two crystallographically independent but chemically identical subunits. The molecular dimensions are approximately 100×63×42 $Å^3$. Each subunit comprises three domains which we label D2, D3 and D4 (Fig. 2). These domains are similar to three of the four domains in the structure of ECAO. The additional N-terminal domain, D1, of ECAO is missing from the PSAO gene: if the ECAO molecule is shaped like a mushroom [4], the two subunits of PSAO form the cap of a mushroom without the stalk. Nevertheless, there is considerable structural homology between the two proteins (Fig. 3). The rms difference between 1178 Cα positions in PSAO and ECAO (inactive form [4]) is 1.4 Å.

The largest domain of each subunit (D4, residues ~227–647) is a β sandwich comprising two twisted anti-parallel β sheets with eight and ten strands, respectively (Fig. 4). The two smaller domains of the subunit, D2 (residues 6–96) and D3 (residues 107–204), lie on the surface of the β sandwich and form an edge of the mushroom cap. Each consists of two helices followed by a slightly curved, anti-parallel, four-stranded β sheet with a β-hairpin turn between strands 3 and 4. Domains D2 and D3 have the same topology and closely similar polypeptide folds at the first helix and the β sheet, and may be described as an 'α/β roll' [17]. They differ with respect to the orientation and contacts of the second helix and the connections between the polypeptide strands.

The active site

The active site has several notable properties. It is buried, and substrate access to it appears to require a substantial rearrangement of the polypeptide; the essential Cu(II) atom and the organic cofactor are close, but not bonded, to each other; and the organic cofactor appears to be highly flexible.

The active site of each subunit is located towards one edge of the β-sandwich domain D4 (Figs 4,5). The Cu atom is coordinated by the imidazole groups of three histidine residues (His442 and His444 at Nϵ2, and His603 at Nδ1) and by two water molecules, one 'equatorial' (O_w652) and one 'axial' (O_w651) (Fig. 6). The coordination geometry is described as approximately square-pyramidal, but at the present resolution the bond angles at the metal atom do not permit an unequivocal distinction between a square-pyramidal and a trigonal-bipyramidal geometry (Table 1). The Cu(II)–ligand bond distances, restrained during the crystallographic refinement to the ranges found in low molecular weight Cu(II) complexes with similar ligands, are consistent with the known $d_{x^2-y^2}$ ground state of the d^9 Cu(II) atom in amine oxidases, as well as with the values found in an extended X-ray absorption fine structure (EXAFS) analysis of PSAO (RA Scott, DMD, unpublished

Figure 2

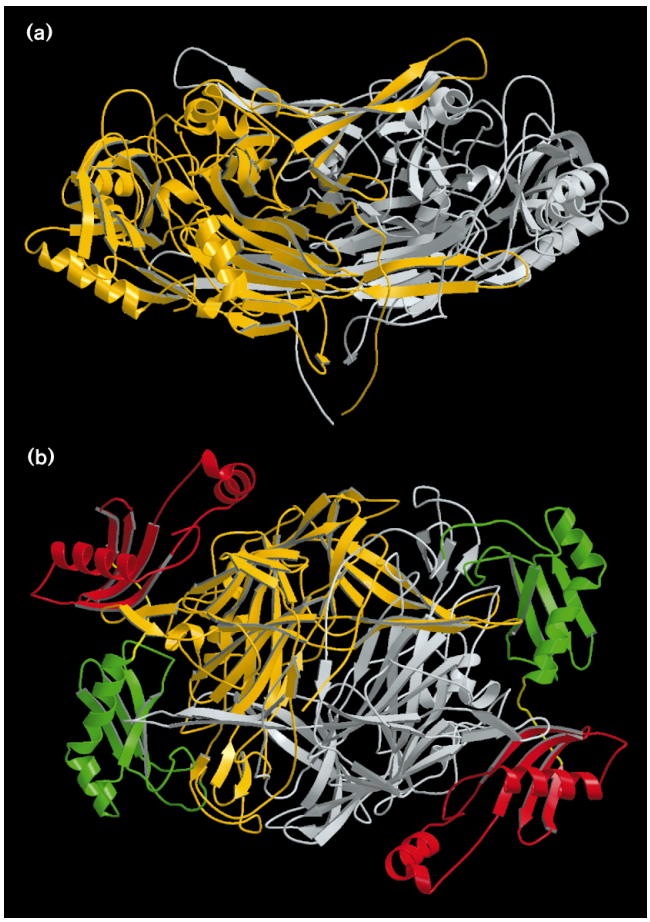

Three-dimensional structure of pea seedling amine oxidase (PSAO). (a) PSAO dimer viewed perpendicular to the molecular dyad axis. The two subunits are in orange and white, respectively. The two β-strand arms which extend from the orange subunit along the surface of the white subunit are seen clearly. (b) PSAO molecule viewed along the molecular dyad axis. The large β-sandwich domain D4 is in orange for one subunit and white for the other, as in (a). Domains D2 and D3 of both subunits are shown in red and green, respectively. An additional N-terminal domain found in *E. coli* amine oxidase is not coded in the PSAO gene. From each D4 domain, a β-strand arm (yellow) extends along the surface of the molecule towards the D3 domain of the other subunit. (Secondary structure assigned using DSSP [48]; figure generated using MOLSCRIPT [49].)

Figure 3

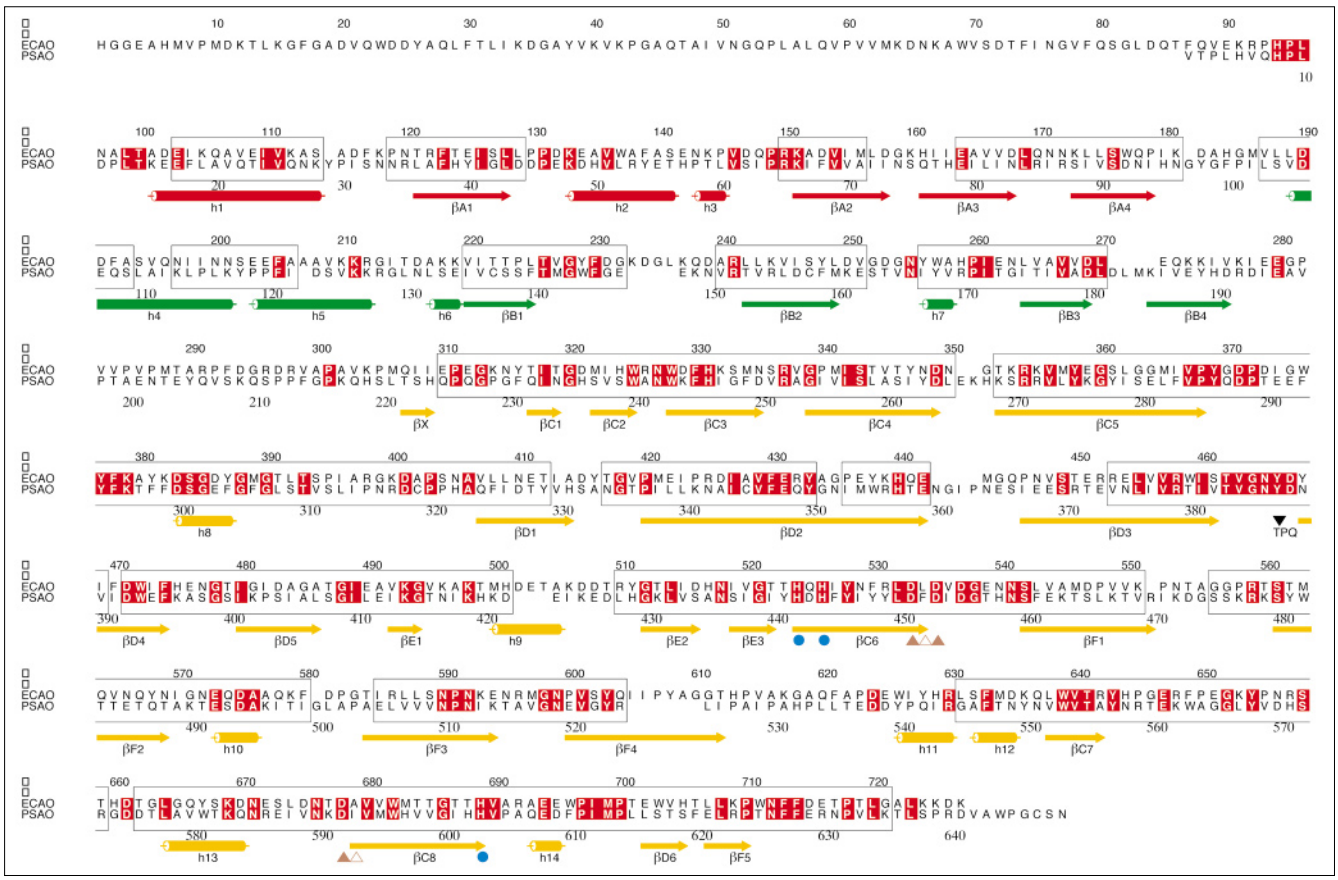

Structure-based sequence alignment of pea seedling and *E. coli* amine oxidases (PSAO, ECAO). Boxes enclose structurally conserved regions (SCRs). The SCRs are defined as those sequences that, when the two structures are superposed, have a rms difference ≤0.7 Å between corresponding Cα positions, and that in addition are displaced with respect to each other by ≤1.2 Å. Identical residues in the SCRs are shown in red. As the only data used in aligning the sequences are derived from the crystal structures, no attempt has been made to optimise the sequence identity outside the SCRs. Cylinders and arrows denote helices and β strands, respectively, in the PSAO structure. The colours correspond to domains: D2, red; D3, green; and D4, orange (as in Fig. 2b). The helices are labelled h and numbered sequentially. The β strands are labelled β and are numbered sequentially according to the β sheet in which they occur (see Fig. 4). The Cu-binding residues are shown as blue circles, the TPQ as an inverted black triangle, and the Mn-binding residues in PSAO as brown triangles, which are solid if Mn bound at the side-chain carboxylate and hollow if Mn bound at the backbone O(peptide). (Secondary structure assigned using DSSP[48]; figure generated using ALSCRIPT [50].)

observations). The two water molecules coordinated to the Cu atom form no hydrogen bonds to protein groups.

The Cu site geometry is in agreement with predictions from X-ray absorption and pulsed electron paramagnetic resonance (EPR) spectroscopy that the Cu(II) atom in amine oxidase has three imidazole ligands [18]. The presence of two modes of imidazole coordination (Nϵ2 and Nδ1) is consistent with indications from pulsed-EPR data [19]. Evidence for both 'equatorial' and 'axial' water ligands was derived from pulsed-EPR and nuclear magnetic relaxation dispersion (NMRD) measurements [19,20]. Furthermore, the absence of hydrogen bonds between the water ligands and the protein may explain the reported lability of the water ligands, at least one of which is in rapid exchange with solvent water despite the fact that it is buried in the protein molecule [20].

The Cu atom and TPQ cofactor are in close proximity (Fig. 6). The position and orientation of the TPQ aromatic group are defined unambiguously (Fig. 7). The quinone oxygen O2 lies approximately 6 Å from the Cu atom and is not coordinated. A small movement of the TPQ aromatic group would be required to facilitate the extremely rapid electron transfer from reduced TPQ to Cu(II) that occurs in PSAO (step 4–5 in Fig. 1) [12]. The TPQ side chain appears to be sufficiently flexible to accommodate this change.

All three oxygen atoms of TPQ are within hydrogen-bonding distances of neighbouring groups. The interatomic

Figure 4

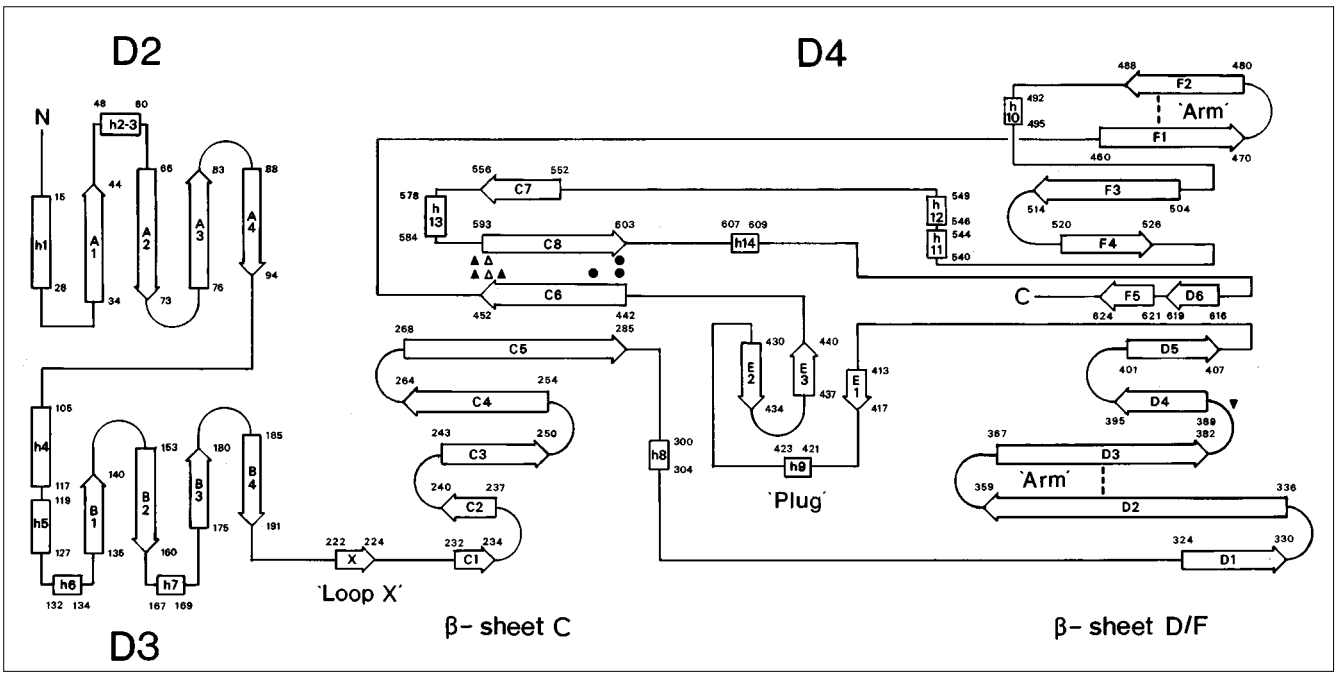

Topological diagram of the PSAO structure. Arrows A–F represent β strands, the length of an arrow being proportional to the number of residues. Boxes, labelled h, represent α or 3_{10} helices. D2, D3 and D4 are the three domains of PSAO as described in the text. The feature labelled 'Plug' lies on the surface of D4, and covers a potential access to the Cu site. The segment labelled 'Loop X' is a three-residue β strand, which interacts with a similar segment in the other subunit to form a small β sheet (seen below the D4 domains in Fig. 2b). The segments labelled 'Arm' extend from one subunit along the surface of the other (see text). (The diagram is drawn in the style of [4] to facilitate comparisons with ECAO.) The histidine residues at the Cu site are denoted by black circles, the TPQ by an inverted black triangle, the aspartic acid residues at the Mn site by black triangles and the residues where Mn is bound at O(peptide) by hollow triangles.

distances are consistent with hydrogen bonds from the quinone oxygen O(2) to the carboxyl group of Asp300, from the hydroxyl oxygen O(4) to the side-chain Nζ atom of Lys296, and from the quinone oxygen O(5) to the hydroxyl group of Tyr286 and the Nδ2 atom of Asn386. Three of these residues — Asp300, Tyr286 and Asn386 — are invariant in all known amine oxidases, whereas the fourth, Lys296, occurs in about half of the known amine oxidase sequences [21]. Inspection of the structure suggests that the hydrogen-bonded interactions have mechanistic significance (see below). It has been noted previously that pulsed-EPR and electron nuclear double resonance (ENDOR) spectroscopic studies of the Cu(I)-semiquinone state are consistent with multiple hydrogen bonds from the protein to the topa semiquinone, and that these may be important in reoxidation of the substrate-reduced enzyme [22].

The role played by the hydrogen bonds from the invariant residues Tyr286 and Asn386 to O(5) is likely to be electrostatic. Recent studies of the oxidation of amines by TPQ models have established that the reactive electrophilic centre of TPQ is at the C(5) carbonyl [9,10]. The two hydrogen bonds at O(5) should enhance the electrophilic nature of C(5), and thus favour the attack of the nucleophilic substrate. Furthermore, a proposed mechanism links substrate attack at the C(5) carbonyl to the abstraction of H^+ by a base, suggested to be a carboxylate with $pK_a \approx 5$ [9,10]. This base can now be identified with high probability as Asp300 (Fig. 1), consistent with the description of the corresponding residue in ECAO (Asp383) as 'a candidate for the base required in the catalytic mechanism' [4]. The presence of a hydrogen bond to the carboxyl group of Asp300 in PSAO implies that this group is protonated in the crystals at pH 4.8, that is, that it has an unusually high pK_a, as required for the proposed mechanism.

The mechanistic significance of the hydrogen bond between Lys296 and the phenolic group of TPQ is also likely to be electrostatic. As mentioned above, Lys296 is not conserved in all amine oxidases. In those, such as PSAO and ECAO, where a residue corresponding to Lys296 is present, the formation of a hydrogen bond to the Lys296 side chain should facilitate the deprotonation of the TPQ phenolic group (pK_a 3.0±0.2). This in turn should favour the formation of a charged reaction intermediate of the type proposed by Klinman and Mu [2]. (In the crystals of PSAO

Figure 5

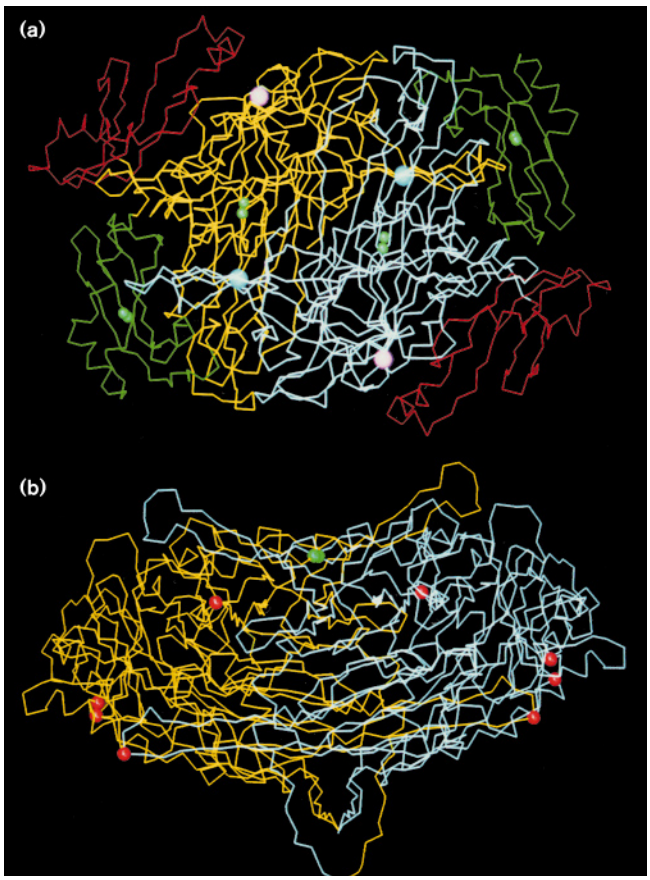

Cα traces of the PSAO dimer. Coloured spheres indicate the locations of selected structural features. The orientations and colour-coding of the polypeptide are the same as in Figure 2. **(a)** Cu atoms (blue), manganese atoms (magenta), and the S atoms of disulfide bridges (green) are highlighted. **(b)** The diagram shows glycosylation sites (red), and the loop corresponding to the heparin-binding site in human amine oxidases (green).

Figure 6

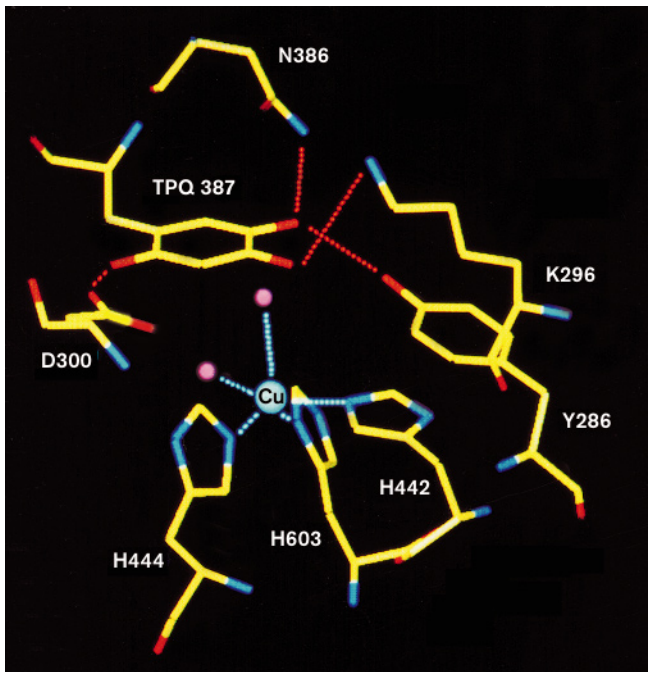

Active site of PSAO, showing the Cu atom (blue sphere), the two coordinated water molecules (magenta spheres), the Cu-binding residues (His442, His444 and His603), the cofactor (TPQ387), and other active-site residues. Hydrogen bonds are shown as dashed red lines.

at pH ~5, the contact identified as a hydrogen bond is in fact likely to be an electrostatic (Lys296)NH_3^+.....$^-$O(TPQ) interaction.) Thus, it is possible that the presence or absence of a residue able to form a hydrogen bond to the phenolic group of TPQ contributes to the observed differences among the kinetics and the catalytic efficiencies of amine oxidases.

Conformational flexibility of the TPQ side chain

There is increasing (but indirect) evidence that the TPQ side chain has considerable flexibility. In the crystals of PSAO, the TPQ atom that makes the closest contact with Asp300 is the quinone oxygen atom O(2). The proposed combination of amine attack at C(5) and H^+ abstraction by Asp300 would require the TPQ to rotate by ~180° about the Cβ–Cγ bond from the orientation observed in the crystals. The picture that emerges is one of a concerted action in which the nucleophilic amine substrate attacks at C(5), the two hydrogen bonds at O(5) (having facilitated that attack and stabilized the orientation of the TPQ) disappear and the aromatic group of the TPQ rotates. A similar degree of mobility is implicit in the substantial change that occurs in the position and orientation of the TPQ side chain when the active form of ECAO is converted to an inactive form [4]. Physical evidence consistent with local mobility is provided by the above-average temperature factors of the TPQ side-chain atoms (~40 Å^2, compared with the molecular average 23 Å^2). Conformational flexibility may also be necessary to meet the dual stereochemical requirements for the oxidation of Tyr387 to TPQ, and the subsequent participation of TPQ in catalysis. As copper is essential for both TPQ biogenesis and catalysis, the question of whether this dual role is associated with structural variations at the Cu site will be a key topic for further study.

Inaccessibility of the active site from the solvent

As might be expected for enzymes that utilize radical chemistry [7], the Cu–TPQ active site is not directly accessible from the solvent. Although it lies close to a surface of the large β-sandwich domain D4, that surface happens to be the interface between the two subunits of the molecule. Access to the Cu site from that direction is therefore impossible. If we assume that it is important to protect

Table 1

Coordination geometry of the copper atom.

Ligand (L) atom	Cu–L bond length (Å)†	Angle (°)†			
		L–Cu–O_w652	L–Cu–Nϵ2(His442)	L–Cu–Nϵ2(His444)	L–Cu–Nδ1(His603)
O_w651	2.5/2.5	67/65	92/99	120/120	103/103
O_w652	2.0/2.0	-	160/164	93/92	91/88
Nϵ2(His442)	2.1/2.2	-	-	99/99	93/95
Nϵ2(His444)	2.1/2.1	-	-	-	135/133
Nδ1(His603)	2.2/2.2	-	-	-	-

†Values are given for the dimensions in subunits A and B, respectively.

radical catalytic intermediates such as the semiquinone shown in Figure 1, then PSAO would not be catalytically competent if it were a monomer.

The most attractive alternative route to the active site is blocked by a β sheet of three short strands (E1–E2–E3), a stretch of seven residues in a partly helical and partly random-coil conformation (residues 421–423, 424–427), and a β-hairpin turn from the other subunit (residues 515–519). In Figure 3 we have labelled the β sheet and helical/random-coil segments as a 'plug', to conform with the description of similar features in the ECAO structure [4]. Inspection of the PSAO model reveals that a movement of the plug would permit a substrate to reach the active site. The required movement might be achieved if Gly409 (an invariant residue) and Gly439 (replaced by alanine or asparagine in some amine oxidases) acted as 'hinges', in which case 'lid' would be a better description than 'plug'. The atoms of the helical/random-coil segment have high temperature factors (~50 $Å^2$), consistent with this region of the polypeptide having additional flexibility.

Interactions between subunits

Most of the interactions between the two subunits occur at the interface between the two β-sandwich domains D4. These domains occupy about half of the molecular volume, and ~36% (7300 $Å^2$) of the surface area of each is buried at the interface between them. They are held together by three types of interaction. First, there are side-chain interactions across the D4–D4 interface. Second, there is a segment of antiparallel β sheet formed by three residues from each subunit (residues 222–224). (In Fig. 2a this segment of β sheet is visible clearly below the body of the molecule.) The residues involved are labelled 'βX' in Figure 3 and 'Loop X' in Figure 4. Third, two remarkable β-ribbon 'arms' extend from each of the D4 domains and embrace the other domain. The arms originate from β-strands D2 and D3 at residues 350–374, and from β-strands F1 and F2 at residues 464–486 (Fig. 4). There are some interesting differences between these arms and analogous features in ECAO [4].

The first arm runs along a groove on the surface of the D4 domain of the other subunit. This arm is approximately 6 Å longer than the corresponding arm in ECAO, enabling residues Glu359, Gly361, Ile362 and Pro363 to make contacts with domain D3 of the other subunit. The carboxyl group of Glu359 is hydrogen-bonded to the phenol group of Tyr168 in domain D3. In the ECAO structure the first arm is not long enough to permit these contacts. The second arm passes within 4 Å of the backbone atoms of the active-site residue His442. A specific intersubunit interaction occurs near the end of this second arm, where the side chain of Trp482 is hydrogen-bonded to the carboxyl group of Asp443, the residue between the two active-site residues His442 and His444 (Fig. 8). In ECAO this interaction is prevented by the fact that the residues corresponding structurally to Trp482 and Asp443 are methionine and glutamate, respectively (Fig. 3), the glutamate being hydrogen-bonded to a backbone oxygen atom in its own subunit.

Two residues at the end of the first arm, Arg356 and His357, are of particular interest because they are linked via hydrogen bonds or salt bridges to several residues close to the Cu site of the other subunit (Fig. 8). The relevant interactions are between the side chains of Arg356 and Asp318, Arg356 and Asp388, His357 and Asp388, and Asp388 and Thr383. Three of these residues are totally conserved (His357, Asp318, Thr383) and two are conservatively substituted (Arg356→Lys, Asp388→Glu) [21].

The reasons for the conservation or conservative substitution of these residues are not yet clear. If PSAO exhibited half-of-the-sites reactivity, as reported for some other amine oxidases [23–25], then it would be reasonable to infer that the links between residues on the arm of one subunit and the active site of the other subunit are connected with an allosteric mechanism. The absence of evidence for half-of-the-sites reactivity in PSAO [26,27] suggests that the network of intersubunit links close to the active site must have a different explanation. In the case of Asp388 (the residue adjacent to the TPQ cofactor, residue 387), the reason why it is conservatively substituted is

Figure 7

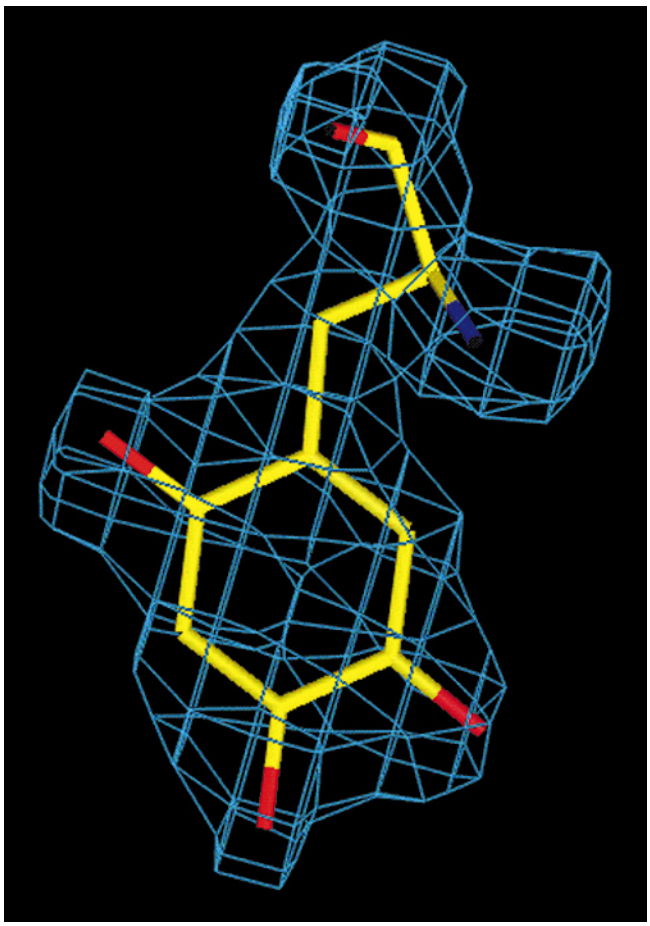

The electron density in an unbiased 'omit' Fourier map defines the quinone oxygen atoms (and hence the orientation of the TPQ side chain) unambiguously. Contours are drawn at the 3.5σ level.

Figure 8

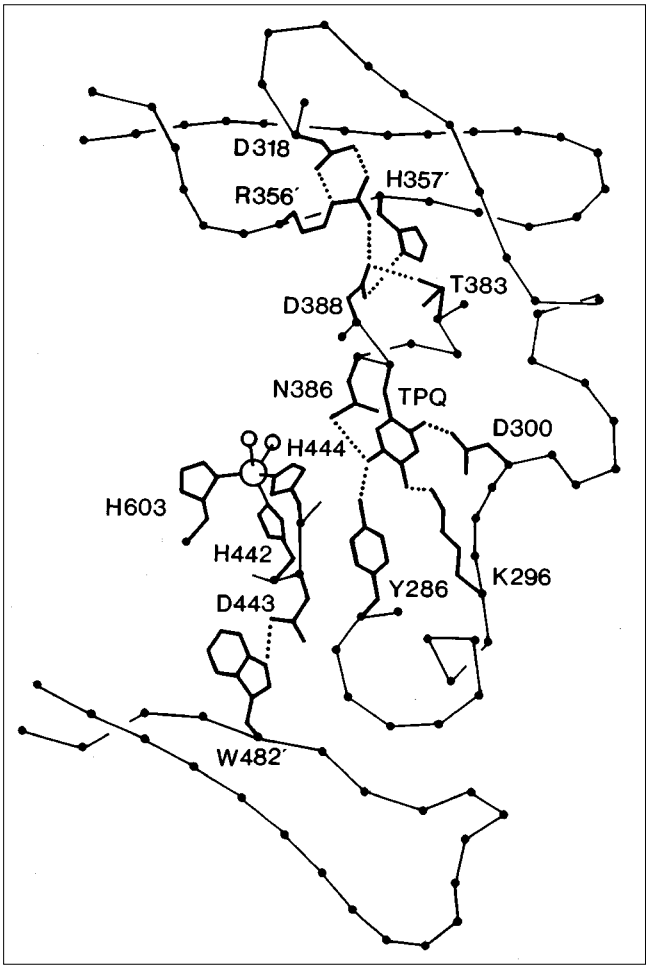

Schematic diagram showing the close relationship between the PSAO active site and the two β-ribbon arms of the other subunit (residues identified by primes). Three of the residues involved in intersubunit links (Asp318, His357′, Thr383) are invariant in all known amine oxidase sequences, and two others (Arg356′, Asp388) are conservatively substituted (see text). The diagram has been adapted from a computer-drawn original by applying small distortions to the functional side chains (heavy lines), hydrogen bonds (broken lines) and polypeptide backbone (Cα atoms joined by light lines).

almost certainly structural rather than mechanistic: yeast amine oxidase remains catalytically active if a glutamate corresponding to Asp388 is mutated to asparagine, showing that the negative charge of the carboxylate group is not essential for catalysis [5].

Cysteine residues, disulfide bridges

The number of cysteine residues differs widely among the amine oxidases that have been sequenced [21]. PSAO has five cysteine residues per subunit (Fig. 5). The formation of two disulfide bridges leaves one free thiol. As neither the disulfides nor the fifth cysteine are close to the metal site, it is unlikely that these groups have any mechanistic role. However an important structural role can be inferred for one of the disulfide bridges, (Cys319)S–S(Cys345), as equivalent residues appear to occur in all eukaryotic amine oxidases, as well as in amine oxidases from some prokaryotes including the gram-positive bacterium *Arthrobacter* [21]. This disulfide bridge occurs in domain D4, linking a residue on a large loop (Cys319) to a residue on β-strand D2 of the β-sheet D/F (Cys345). The other disulfide bridge, (Cys137)S–S(Cys158), makes a link between two of the β strands in domain D2. The residues involved are not conserved [21] so that the link is unlikely to be of general significance.

The two disulfides account for four of the five cysteines in each subunit of the PSAO structure. The fifth cysteine, Cys647, is located two residues before the C terminus, and is not well ordered in the crystal structure (see 'Model building and structure refinement', below). Titrations of substrate-reduced PSAO with a variety of thiol reagents have so far failed to provide evidence for a free cysteine

(KA McKeown, DMD, unpublished observations). Reports of a titratable cysteine associated with substrate reduction in other amine oxidases [14,15,28] may refer to residues that are not conserved in PSAO. The lack of a detectable free cysteine in PSAO would be rationalized by the formation of an intersubunit disulfide bond. The evidence for disorder at the three C-terminal residues is inconsistent with the presence of such a bond in the present structure but the cysteines of the two subunits could be brought within S–S bonding distance if the configuration at Pro645 is changed from *trans* to *cis*. The possibility that this occurs, particularly following partial unfolding, has not been eliminated.

Glycosylation sites

PSAO has four potential glycosylation sites (Asn131–Leu–Ser, Asn334–Gly–Thr, Asn364–Glu–Ser and Asn558–Arg–Thr). Asn131 belongs to domain D3, Asn334 and Asn558 to domain D4, and Asn364 to one of the 'arms' from the other subunit. All four sites are located on the surface of the molecule (Fig. 5a), so that deglycosylation or mutagenesis of the asparagine residues would be unlikely to disrupt the structure. Two sugar residues at the Asn131 site and one sugar residue at the Asn558 site are sufficiently well ordered to be identified unequivocally in electron-density maps. Weaker electron density that may correspond to a sugar group is observed at Asn334 in one subunit but not in the other. There is no evidence for sugar residues at the Asn364 site.

Tentative identification of a heparin-binding site in human amine oxidase

The recent discovery that human amine oxidase sequences have a consensus binding site for the anionic polysaccharide heparin [29] raises intriguing questions concerning the functional significance of heparin–amine oxidase interactions. Heparin, a negatively charged polysaccharide, binds to a variety of proteins. It has the effect of mediating protein–protein interactions, including some that occur in blood clotting. Protein–protein interactions that are modulated by heparin may occur at the cell surface, in the extracellular matrix of tissues, and in the serum. The consensus heparin-binding motif in human amine oxidases is Arg–Phe–Lys–Arg–Lys–Leu–Pro–Lys [29]. In a published sequence alignment [21], this eight-residue segment in human amine oxidases corresponds (but without sequence identity) to residues 500–507 in PSAO. Residues 500–507 lie on a solvent-exposed loop at the bottom of a shallow depression near the centre of domain D4 (Fig. 5a). By analogy, we tentatively identify this loop as the heparin-binding site in human amine oxidases. In PSAO, the loop lies between two regions where the PSAO and ECAO molecules are sufficiently similar to be described as 'structurally conserved' (Fig. 3). Pending the structure analysis of other amine oxidases, we suggest that the location of the loop in relation to the rest of the molecule is likely to be conserved, even though the length, conformation and amino-acid sequence of the loop may well be different from protein to protein.

The second metal site

The crystal structure of PSAO has revealed a second, octahedral metal-binding site (Fig. 9). The ligands are the carboxylate groups of Asp451, Asp453 and Asp592, the peptide carbonyl oxygens of Phe452 and Ile593, and a water molecule. Two of the coordinated asparagine residues, Asp451 and Asp592, are strictly conserved. The third, Asp453, occurs in the majority of amine oxidase sequences (the current exceptions being *Arthrobacter globoformis*, *Arthrobacter P1* and *Hansenula polymorpha*) [21]. The location of this second metal site is shown in Figure 5b. The five coordinating residues lie on the same two β strands as the three histidine residues that coordinate the Cu atom (Figs. 3,4). The distance from the Cu site, ~33 Å, does not exclude the possibility that the second metal site has a regulatory role. This hypothesis has not been explored experimentally.

The electron density associated with the second metal site is lower than that at the Cu site. We have modeled it as manganese, which is consistent with a variety of observations on eukaryotic amine oxidases. Specifically, Mn(II) is frequently observed in highly purified PSAO preparations, being identified by its characteristic EPR signal. The Mn(II) can be removed readily (as inferred from the

Figure 9

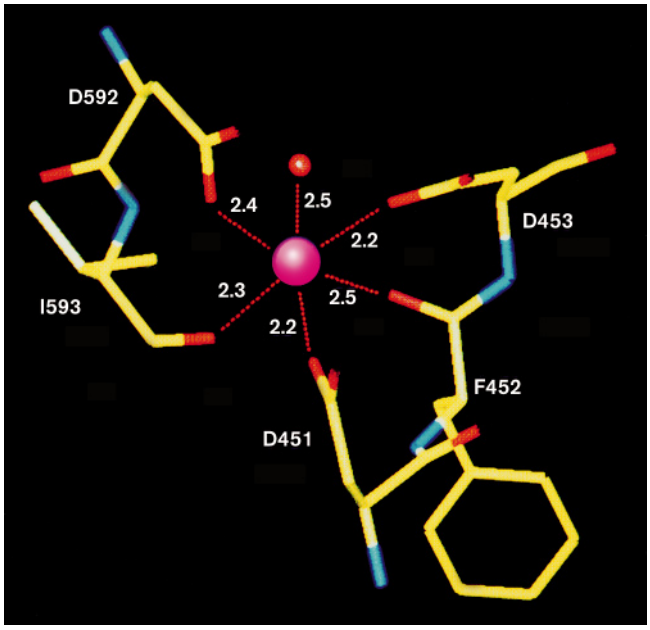

Coordination geometry and ligands of the second metal atom in PSAO (tentatively identified as Mn). A coordinated water molecule is shown as a small red sphere. The second metal site is connected to the Cu site by two β strands (see Fig. 4). A similar metal site occurs in ECAO [4].

loss of the Mn(II) EPR signal) by dialysis against EDTA-containing buffers, without affecting the PSAO activity (DMD, unpublished observations). It is likely that other amine oxidases with aspartic acid residues equivalent to those in PSAO also have a second metal site that may be occupied by Mn(II). For example, the human placental enzyme, in which all three aspartic acid residues of the second metal site in PSAO are conserved, was originally reported as a Cu(II)Mn(II) metalloprotein, owing to the presence of bound Mn(II) that resisted removal by Chelex-column chromatography [30]. An identical site occurs in the crystal structure of ECAO, and the possibility that this site is occupied by Mn(II), Ca(II) or Mg(II) under physiological conditions has been indicated [4].

Biological implications

Copper-containing amine oxidases catalyze the oxidative deamination of primary amines. The first crystal structure for this class of enzyme — of an *E. coli* amine oxidase — was solved only recently. This paper describes the first structure of a eukaryotic copper-containing amine oxidase, pea seedling amine oxidase (PSAO). In plants, these enzymes are implicated in cell-wall biosynthesis, wound response, and in the synthesis of certain growth factors. In other eukaryotes, copper-containing amine oxidases are thought to be involved in a wide variety of physiological processes, including the regulation of biogenic amine concentrations, and the control of cell growth and differentiation. The PSAO structure is expected to provide a useful basis for modeling the structures of mammalian amine oxidases, including the human enzymes, which may prove to be attractive targets for the structure-based design of therapeutic agents.

The structure of PSAO is remarkably similar to that of the prokaryotic *E. coli* amine oxidase (ECAO) [4], even though the level of sequence identity in a published alignment is only 23% [21]. The active site of both proteins comprises a Cu(II) atom coordinated by three histidine side chains and two water molecules, and a 2,4,5-trihydroxyphenylalanine quinone (TPQ) cofactor. The Cu(II) atom has a distorted square-pyramidal geometry. The coordinating groups and the coordination geometry are consistent with extensive spectroscopic results, and are well precedented for Cu(II). The TPQ cofactor (derived via post-translational modification of a tyrosine residue) is well resolved in the PSAO electron-density maps. The TPQ aromatic group is located about 6 Å from the Cu atom. Its position in relation to the Cu atom is different from that in the inactive form of ECAO, and its orientation is different from that in the active form of ECAO [4]. These comparisons suggest that the TPQ side chain is highly mobile within the active site.

Amine oxidases may be examples of enzymes where the dynamics of conformational change, both within the active site and at the protein surface, are important in catalysis. Firstly, the extremely high rate of electron transfer between reduced TPQ and Cu(II), required to generate the Cu(I)-semiquinone state which is proposed to be a key catalytic intermediate, is consistent not only with the proximity of the TPQ to the Cu atom but also with the hypothesis that the TPQ side chain has a flexible conformation. Secondly, it seems likely that the catalytic oxidation of amines and the biogenesis of TPQ require the phenolic ring to be in different positions and orientations with respect to the Cu atom. This provides yet another reason why the side chain of TPQ (and, by implication, its tyrosine precursor) must be flexible. Finally, as there is no unobstructed access to the active site, the binding of a substrate molecule depends in part on the dynamics of conformational changes at the surface of the molecule.

The structure analysis of the pea seedling enzyme has identified the location of a disulfide bridge that is conserved among eukaryotes, as well as potential glycosylation sites. A second metal site, which rationalizes previous observations of exogenous metal (particularly Mn) binding to eukaryotic amine oxidases, has also been identified. The extensive and unusual contacts between the subunits in the dimer, first revealed in the ECAO structure, are remarkably conserved in the PSAO structure. A reasonable hypothesis is that other amine oxidases have similar intersubunit links. However, such links should not be invoked to explain the persistent reports of negative cooperativity in some eukaryotic amine oxidases [23–25]. There is no evidence that PSAO, where the unusual intersubunit contacts certainly exist, exhibits negative cooperativity [26,27].

Materials and methods

Crystallization and data collection

PSAO, purified as described in [27], was crystallized using 1.44 M lithium sulfate at pH 4.8 as precipitant [16]. Crystals were grown by macroseeding sitting drops. The observed symmetry and systematic absences identified the space group as orthorhombic $P2_12_12_1$. The average cell dimensions a=85.4(1), b=114.6(4), c=199.9(8) Å were found by averaging the refined values from 74 image-plate records. The crystallographic characterization of the native protein and potential heavy-atom derivatives was carried out on a MarResearch image-plate detector on beamline 7–1 at the Stanford Synchrotron Radiation Laboratory; Weissenberg image-plate cameras on beamlines 6A2 and 18B at the Photon Factory, Tsukuba; and an in-house Rigaku R-axis IIc detector on a rotating-anode generator.

Extensive trials yielded only one useful isomorphous heavy-atom derivative. This derivative was prepared from phosphotungstic acid ($H_3PW_{12}O_{40}$). All other attempts to prepare heavy-atom derivatives for MIR phasing by soaking/co-crystallization were unsuccessful, due to non-isomorphism or lack of substitution. The native protein crystals were unstable at low salt concentrations and at pH≥6, so that conditions that might have been more conducive to heavy-atom binding could not be explored.

Diffraction intensity data for the native protein and the phosphotungstate derivative were recorded on a Weissenberg camera [31] on beamline 18B at the Photon Factory, Tsukuba, Japan (ω-scans, 400×200 mm^2

image plates, crystal-plate distance 430 mm). The data for the native protein were recorded at λ=1.00 Å from two crystals, using two image plates for each exposure. The data for the phosphotungstate derivative were recorded at λ=1.07 Å, i.e. just below the tungsten LII absorption edge at 1.074 Å (where f′= –12.2915, f″=8.3015). Only a single image plate was used for each exposure, yielding limited data in the resolution range 4.5–2.7 Å (Table 2).

The image-plate data were processed, scaled and merged using the programs DENZO and SCALEPACK [32]. All the observations, including those with negative intensities, were used for scaling and merging. For the phosphotungstate derivative data, Bijvoet-related reflections were treated as equivalent for scaling but were processed separately during merging. The statistics of data collection are shown in Table 2.

Structure determination

The hypothesis that the asymmetric unit of PSAO is a dimer with M_r ~145 000 Da led to a reasonable value, 3.37 $Å^3Da^{-1}$, for the Matthews coefficient V_m [33]. The highest non-origin peak in a self-rotation function was half as high as the origin peak and occurred at polar coordinates ϕ=90º, φ=6.5º, κ=180º. This peak was equivalent to a molecular dyad aligned almost parallel to a crystallographic axis (010 direction), as frequently observed in this space group [34].

Initial attempts to use the phosphotungstate derivative were unrewarding. The positions of the W_{12} clusters – one cluster per protein subunit – were obtained by a Patterson analysis using the program HASSP [35]. However, protein phases calculated by treating the W_{12} clusters as a point-scatterer were limited to 5 Å with a poor figure of merit (~0.28).

The additional phase information required to solve the structure was obtained by molecular replacement (MR). The program used for the MR calculations was AMoRe [36]. This and the programs DM, MLPHARE and PROLSQ mentioned later were used as the CCP4 versions [37]. The most successful search model comprised a truncated version of the ECAO molecule (residues 99–699 of both subunits, side chains omitted beyond Cβ, all B factors =15 $Å^2$). The rotation search was carried out by real-space as well as reciprocal-space methods. A convincing MR solution was obtained. In the rotation function, the highest peak was twice as high as the second highest, and was subsequently shown to be the correct solution. In the translation function, the highest peak was also the correct solution (correlation coefficient 14.5%, residual 54%), compared with the highest noise peak (correlation coefficient 8.3%, residual 56%). The interpretation of Fourier maps computed with the MR phases was prevented by the absence of sufficient electron-density features for the identification of side chains. Moreover, when Fourier maps were computed using phases from the truncated ECAO molecule further reduced by the omission of 10-residue polypeptide segments, the density corresponding to the omitted residues did not appear. This confirmed the inadequate phasing power of the model.

Though the phases obtained by MR were not sufficient to solve the PSAO structure directly, difference Fourier maps calculated with these phases and with the differences between the native and phosphotungstate derivative amplitudes did reveal hollow spheres of electron density. The positions of these spheres were consistent with the sites of the two W_{12} clusters deduced from the original difference Patterson maps. The known atomic coordinates of a phosphotungstate ($PW_{12}O_{40}^{3}$) ion [38] could be fitted into the electron-density difference maps derived from the MR phases. The 24 W sites thus obtained were refined for position and occupancy, each W atom being assigned a fixed B-value of 15 $Å^2$. The refined tungsten parameters were then used to calculate a set of SIROAS (single isomorphous replacement and optimized anomalous scattering) protein phases at 2.7 Å resolution. The refinement of the W atom positions and the SIROAS phasing were carried out by means of MLPHARE [39]). Despite the low R_{deriv} (9.9%) and the limited number of data, the phosphotungstate derivative proved to be exceptionally effective (overall phasing power 2.2, average figure of merit 0.46) (Table 3). After solvent flattening, the electron-density maps clearly showed the molecular boundary, the polypeptide segments bearing the copper ligands, and several β-strands and helices.

The SIROAS phases were further improved by 40 cycles of solvent flattening, histogram matching, and twofold non-crystallographic symmetry averaging, using DM [40]). The initial free residual R, 56.2% for 5% of the data, dropped to 23.0% by the end of the phase-improvement cycles. The electron-density maps computed with improved phases were readily interpretable, and an almost complete molecule of PSAO

Table 2

Statistics of data collection.

	Native protein	$PW_{12}O_{40}$ derivative
Wavelength (Å)	1.00	1.07
No. of crystals	2	1
No. of observations	683 441	161272
No. of unique reflections	86 780	38 026
d_{min} (Å)	2.2	2.7
Completeness (%)	86.5	70.0
R_{merge} (%)*	5.9	4.1
R_{anom} (%)†	-	3.3
Completeness (%)‡		
Resolution >4.5 Å	96.5	95.7
4.5–3.5 Å	96.5	81.1
3.5–3.0 Å	93.4	62.5
3.0–2.7 Å	91.0	43.8
2.7–2.5 Å	88.6	-
2.5–2.3 Å	86.2	-
2.3–2.2 Å	55.1	-

*$R_{merge}=\Sigma|I-\langle I\rangle|/\Sigma\langle I\rangle$, where the summation is over all the equivalent measurements including Friedel pairs. †$R_{anom}=\Sigma|\langle I^+\rangle-\langle I^-\rangle|/\Sigma(\langle I^+\rangle+\langle I^-\rangle)$, where I^+ and I^- are Friedel pairs. ‡Data with $F/\sigma(F)\geq 1.0$.

Table 3

Phasing statistics for $PW_{12}O_{40}$ derivative.

No. of $PW_{12}O_{40}$ clusters per dimer	2
R_{deriv} (%)*	9.9
R_{cullis} for centric reflections (%)†	46
R_{cullis} for acentric reflections (%)†	59
Heavy-atom contribution‡	
Resolution >9.5 Å	2.90, 0.59
9.5–7.1 Å	2.45, 0.50
7.1–5.5 Å	2.11, 0.43
5.5–4.6 Å	2.38, 0.49
4.6–3.9 Å	2.09, 0.47
3.9–3.4 Å	1.95, 0.45
3.4–3.0 Å	2.06, 0.42
3.0–2.7 Å	2.36, 0.47
Overall	2.19, 0.46

*$R_{deriv}=\Sigma|F_{PH}-F_P|/\Sigma|F_P|$, where F_{PH} and F_P are the structure amplitudes of the heavy-atom derivative and the native protein, respectively. †$R_{cullis}=\Sigma|F_{PH}-F_P|-|F_{H(calc)}|/\Sigma|F_{PH}-F_P|$, where $F_{H(calc)}$ are calculated heavy atom structure factors. ‡Values given correspond to the phasing power and figure of merit, respectively. Phasing power is defined as $\langle F_H\rangle/\langle E\rangle$, where $\langle F_H\rangle$ is the mean structure factor amplitude of the heavy atoms and $\langle E\rangle$ is the mean closure error.

could be built into these maps. General agreement with the ECAO structure was taken as confirming the connectivity.

Model building and structure refinement
The polyalanine model from the MR solution was used as a template for the atomic model wherever it was in agreement with the electron density. Other polypeptide segments were built from the skeletonized electron density using BONES atoms. A library derived from well refined structures in the Protein Data Bank was used extensively to model loop segments and side-chain atoms into the electron density.

The structure was refined by a combination of restrained least-squares (PROLSQ [41]) and two cycles of simulated annealing/molecular dynamics (X-PLOR [42]), with intermittent computer-graphics adjustment (O [43]). The Fourier maps were computed using weighted coefficients and model phases [44]. In order to reduce model bias, the model was subjected to restrained least-squares refinement prior to all 'omit' map calculations. The refinement commenced at 2.7 Å resolution with an overall B value. The initial seven cycles of least-squares were followed by simulated annealing refinement (heat stage 4000 K, 25 K temperature decrement every 25 fs). The diffraction data were extended in steps until all reflections to 2.2 Å with $F/\sigma(F) \geq 1.0$ were included. The refinement of individual isotropic B values and the addition of solvent molecules to the model commenced when the phases had been extended to 2.5 Å resolution. Tight stereochemical restraints between the two crystallographically independent subunits were applied during the initial stages of refinement, but were switched off when the data to 2.4 Å resolution were included in the refinement.

The Cu site geometry and the conformation of the TPQ side chain were confirmed by means of 'unbiased' omit maps. Throughout the least-squares refinement, the Cu–ligand bond lengths were restrained to values taken from square-pyramidal low-molecular-weight Cu(II) complexes (Cu–N(imidazole), 2.1 Å; Cu–$O_{equatorial}$, 2.0 Å; Cu–O_{axial}, 2.6 Å). The axial coordination position was assigned to the water ligand O_W651. Unrestrained refinement led to an implausible value, 1.7 Å, for the axial Cu–O bond, but did not affect the other Cu-site dimensions significantly. It was noted that the bond angles at the Cu atom (Table 1) agree equally well with trigonal-bipyramidal coordination, if O_W652 and Nε2(His442) are treated as axial ligands. When the final refinement cycles were repeated with distance restraints appropriate for trigonal-bipyramidal coordination, the bond angles at the Cu atom did not change significantly. A similar ambiguity in the Cu-site geometry was reported for ECAO [4].

Except for a few residues near the N and C termini, and the side-chain atoms of a few solvent-exposed residues, most of the residues could ultimately be built into the electron-density maps. (No density was observed for the five N-terminal and two C-terminal residues. Weak electron density and high B values were observed for Pro58–Thr59–Leu60, Gly646–Cys647, and side-chain atoms of Arg53(B), Lys126(A), Glu148(B), Lys149(A), Lys425, Glu426, Lys472 and Arg640(B), where A and B denote that the electron density was weak in only one of the two subunits.)

Quality of the structure
The final PSAO model comprises 1282 amino-acid residues and 584 other groups (the TPQ cofactor, two metal atoms and three *N*-acetylglucosamine moieties in each subunit, plus solvent molecules). The residual R is 18.1 % for all reflections with $F/\sigma(F) \geq 1.0$ in the resolution range $7.0 \geq d \geq 2.2$ Å. The maximum average error estimated from a Luzzati plot [45] is ~0.2 Å.

The stereochemistry is satisfactory (Table 4). In a Ramachandran plot (not shown), the only residue in both subunits that lies outside the energetically allowed regions is Ala241. This residue occupies a position that is normally occupied by a glycine (position 2 of a type-II′ turn). The rms difference between corresponding Cα atoms of the independent subunits is 0.16 Å, and a $\Delta\phi/\Delta\varphi$ plot [46] is featureless, leading to the inference that the refinement strategy has not led to 'over-fitting' of the structure [47].

Table 4

Stereochemical parameters.*

	Parameter value	Typical value
Resolution (Å)	2.2	
No. of non-hydrogen atoms	10 939	
Main-chain parameters†		
Residues in core φ,ψ region (%)	87.1	80.5
S.d. of peptide-bond planarity (ω) (°)	4.9	6.0
S.d. of Cα tetrahedral distortion (ζ) (°)	2.9	3.1
Side-chain torsion angles†		
S.d. of χ_1 (*gauche*$^+$) (°)	14.3	19.4
S.d. of χ_1 (*gauche*$^-$) (°)	13.7	20.4
S.d. of χ_1 (*trans*) (°)	15.6	21.8
Other criteria†		
Bad contacts per 100 residues	0.5	7.0
S.d. of hydrogen-bond energies (kJ mol^{-1})	0.9	0.9

*Values in the present work are compared with typical values from a database of known structures, using PROCHECK [51]. †S.d. represents the standard deviation.

Accession number
The atomic coordinates have been deposited in the Brookhaven Protein Data Bank.

Acknowledgements

We thank Professor SEV Phillips, Dr PF Knowles, Dr M McPherson and their colleagues at the University of Leeds for making the atomic coordinates for ECAO available prior to publication, as well as for helpful discussions. The research was supported by the Australian Research Council (Grant. No. A29230677 to HCF and JMG) and the National Institutes of Health (Grant No. GM27659 to DMD). Travel to the Photon Factory and the Stanford Synchrotron Radiation Laboratory was assisted by grants from the Australian Nuclear Science & Technology Organisation and the Dr Joan R Clark Research Fund. Access to Professor N Sakabe's data-collection facilities at the Photon Factory is gratefully acknowledged. The Stanford Synchrotron Radiation Laboratory is supported by the US Department of Energy, Office of Basic Research, and the Division of Research Resources of the National Institutes of Health.

References

1. McIntire, W.S. & Hartmann, C. (1993). Copper-containing amine oxidases. In *Principles and Applications of Quinoproteins* (Davidson, V.L., ed), pp. 97–171, Marcel Dekker, NY, USA.
2. Klinman, J.P. & Mu, D. (1994). Quinoenzymes in biology. *Annu. Rev. Biochem.* 63, 299–344.
3. Knowles, P.F. & Dooley, D.M. (1994). Amine oxidases. In *Metal Ions in Biological Systems* (Sigel, H. & Sigel, A., eds), vol. 30, pp. 361–403, Marcel Dekker, NY, USA.
4. Parsons, M.R., *et al.*, & Knowles, P.F. (1995). Crystal structure of a quinoenzyme: copper amine oxidase of *Escherichia coli* at 2 Å resolution. *Structure* 3, 1171–1184.
5. Cai, D. & Klinman, J.P. (1994). Evidence for a self-catalytic mechanism of 2,4,5–trihydroxyphenylalanine quinone biogenesis in yeast copper amine oxidase. *J. Biol. Chem.* 269, 32039–32042.
6. Matsuzaki, R., Fukui, T., Sato, H., Ozaki, Y. & Tanizawa, K. (1994). Generation of the topa quinone cofactor in bacterial monoamine oxidase by cupric-ion dependent autoxidation of a specific tyrosyl residue. *FEBS Lett.* 351, 360–364.
7. Fontecave, M. & Eklund, H. (1995). Copper amine oxidase: a novel use for a tyrosine. *Structure* 3, 1127–1129.

8. Dooley, D.M. (1994). Commentary on: copper amine oxidase. *Chemtracts - Inorganic Chemistry* 6, 114–120.
9. Mure, M. & Klinman, J.P. (1995). Model studies of topaquinone-dependent amine oxidases. 1. Oxidation of benzylamine by topaquinone analogs. *J. Am. Chem. Soc.* 117, 8698–8718.
10. Mure, M. & Klinman, J.P. (1995). Model studies of topaquinone-dependent amine oxidases. 2. Characterization of reaction intermediates and mechanism. *J. Am. Chem. Soc.* 117, 8707–8718.
11. Dooley, D.M., McGuirl, M.A., Brown, D.E., Turowski, P.N., McIntire, W.S. & Knowles, P.F. (1991). A Cu(I)-semiquinone state in substrate-reduced amine oxidases. *Nature* 349, 262–264.
12. Turowski, P.N., McGuirl, M.A. & Dooley, D.M. (1993). Intramolecular electron transfer between active-site copper and topa quinone in pea seedling amine oxidase. *J. Biol. Chem.* 268, 17680–17682.
13. Dooley, D.M. & Brown, D.E. (1996). Intramolecular electron transfer in the oxidation of amines by methylamine oxidase from *Arthrobacter* P1. *J. Biol. Inorg. Chem.*, in press.
14. Floris, G., Giartosio, A. & Rinaldi, A. (1983). Essential sulfhydryl groups in diamine oxidase from *Euphorbia characias* latex. *Arch. Biochem. Biophys.* 220, 623–627.
15. Zeidan, H., Watanabe, K., Piette, L.H. & Yasunobu, K.T. (1980). Electron spin resonance studies of plasma amine oxidase. Probing of the environment about the substrate-liberated sulfhydryl groups in the active site. *J. Biol. Chem.* 255, 7621–7626.
16. Vignevich, V., Dooley, D.M., Guss, J.M., Harvey, I., McGuirl, M.A. & Freeman, H.C. (1993). Crystallization and preliminary crystallographic characterization of the copper-containing amine oxidase from pea seedlings. *J. Mol. Biol.* 229, 243–245.
17. Orengo, C.A. & Thornton, J.M. (1993). Alpha plus beta folds revisited: some favoured motifs. *Structure* 1, 105–120.
18. Scott, R.A. & Dooley, D.M. (1985). X-ray absorption spectroscopic studies of the copper(II) sites in bovine plasma amine oxidase. *J. Am. Chem. Soc.* 107, 4348–4350.
19. McCracken, J., Peisach, J. & Dooley, D.M. (1987). Cu(II) coordination chemistry of amine oxidases: pulsed electron paramagnetic resonance studies of histidine imidazole, water, and exogenous ligand coordination. *J. Am. Chem. Soc.* 109, 4064–4072.
20. Dooley, D.M., *et al.*, & Koenig, S.H. (1991). Coordination chemistry of copper-containing amine oxidases: nuclear magnetic relaxation dispersion studies of copper binding, solvent-water exchange, substrate and inhibitor binding, and protein aggregation. *J. Am. Chem. Soc.* 113, 754–762.
21. Tipping, A.J. & McPherson, M.J. (1995). Cloning and molecular analysis of the pea seedling copper amine oxidase. *J. Biol. Chem.* 270, 16939–16946.
22. Warncke, K., Babcock, G.T., Dooley, D.M., McGuirl, M.A. & McCracken, J. (1994). Structure of topa-semiquinone catalytic intermediate of amine oxidase as revealed by magnetic interactions with exchangeable ^{2}H and ^{1}H nuclei. *J. Am. Chem. Soc.* 116, 4028–4037.
23. Morpurgo, L., *et al.*, & Avigliano, L. (1988). Spectroscopic studies of the reaction between bovine serum amine oxidase (copper-containing) and some hydrazides and hydrazines. *Biochem. J.* 256, 565–570.
24. Collison, D., *et al.*, & McGuirl, M.A. (1989). Studies on the active site of pig plasma amine oxidase. *Biochem. J.* 264, 663–669.
25. De Biase, D., Agostinelli, E., De Matteis, G., Mondovi, B. & Morpurgo, L. (1996). Half-of-the-sites reactivity of bovine serum amine oxidase. Reactivity and chemical identity of the second site. *Eur. J. Biochem.* 237, 93–99.
26. Padiglia, A., Medda, R. & Floris, G. (1992). Lentil seedling amine oxidase: Interaction with carbonyl reagents. *Biochem. Int.* 28, 1097–1107.
27. McGuirl, M.A., McCahon, C.D., McKeown, K.A. & Dooley, D.M. (1994). Purification and characterization of pea seedling amine oxidase for crystallization studies. *Plant Physiol.* 106, 1205–1211.
28. Suva, R.H. & Abeles, R.H. (1978). Studies on the mechanism of plasma amine oxidase. *Biochemistry*, 17, 3538–3545.
29. Novotny, W.F., Chassande, O., Baker, M., Ladzunski, M. & Barbry, P. (1994). Diamine oxidase is the amiloride-binding protein and is inhibited by amiloride analogues. *J. Biol. Chem.* 269, 9921–9925.
30. Crabbe, M.J.C., Waight, R.D., Bardsley, W.G., Barker, R.W., Kelly, I.D. & Knowles, P.F. (1976). Human placental diamine oxidase. Improved purification and characterization of a copper- and manganese-containing amine oxidase with novel substrate specificity. *Biochem. J.* 155, 679–687.
31. Sakabe, N. (1991). X-ray diffraction data collection system for modern protein crystallography with a Weissenberg camera and an imaging plate using synchrotron radiation. *Nucl. Instr. Methods Phys. Res., Sect. A* 303, 448–463.
32. Otwinowski, Z. (1993). Oscillation data reduction program. In *Proceedings of the CCP4 Study Weekend: Data Collection and Processing* (Sawyer, L., Isaacs, N. & Bailey, S.S., eds), pp. 56–62, SERC Daresbury Laboratory, Warrington, UK.
33. Matthews, B.W. (1968). Solvent content of protein crystals. *J. Mol. Biol.* 33, 491–497.
34. Wang, X. & Janin, J. (1993). Orientation of non-crystallographic symmetry axes in protein crystals. *Acta Cryst. D* 49, 505–512.
35. Terwilliger, T.C., Kim, S.-U. & Eisenberg, D. (1987). Generalized method of determining heavy-atom positions using the difference Patterson function. *Acta Cryst. A* 43, 1–5.
36. Navaza, J. (1994). AMoRe: an automated package for molecular replacement. *Acta Cryst. A* 50, 157–163.
37. Collaborative Computational Project, Number 4. (1994). The CCP4 suite: programs for protein crystallography. *Acta Cryst. D* 50, 760–763.
38. Ouahab, L. & Grandjean, D. (1991). Structure of tris(3,3',4,4'-tetramethyl- 2,2',5,5'-tetraselenafulvalenium)phosphotungstate: $(TMTSF)_3PW_{12}O_{40}$. *Acta Cryst. C* 47, 2670–2672.
39. Otwinowski, Z. (1991). Maximum likelihood refinement of heavy atom parameters. In *Proceedings of the CCP4 Study Weekend: Isomorphous Replacement and Anomalous Scattering* (Wolf, W., Evans, P.R. & Leslie, A.G.W., eds), pp. 80–86, SERC Daresbury Laboratory, Warrington, UK.
40. Cowtan, K. (1994). DM: an automated procedure for phase improvement by density modification. In *Joint CCP4 and ESF-EACBM Newsletter on Protein Crystallography*, No. 31, pp. 34–38, SERC Daresbury Laboratory, Warrington, UK.
41. Hendrickson, W.A. & Konnert, J.H. (1980). Incorporation of stereochemical information into crystallographic refinement. In *Computing in Crystallography* (Diamond, R., Ramaseshan, S. & Venkatesan, K., eds), pp. 13.01–13.23, Indian Academy of Sciences, Bangalore, India.
42. Brünger, A.T., Krukowski, A. & Erickson, J. (1990). Slow-cooling protocol for crystallographic refinement by simulated annealing. *Acta Cryst. A* 46, 583–593.
43. Jones, T.A., Zou, J.Y., Cowan, S.W. & Kjeldgaard, M. (1991). Improved methods for building models in electron density maps and the location of errors in the model. *Acta Cryst. A* 47, 110–119.
44. Read, R.J. (1986). Improved Fourier coefficients for maps using phases from partial structures with errors. *Acta Cryst. A* 42, 140–149.
45. Luzatti, V. (1952). Traitement statistique des erreurs dans la détermination des structures cristallines. *Acta Cryst.* 5, 802–810.
46. Korn, A.P. & Rose, D.R. (1994). Torsion angle differences as a means of pinpointing local polypeptide chain trajectory changes for identical proteins in different conformational states. *Protein Eng.* 7, 961–967.
47. Kleywegt, G.J. & Jones, T.A. (1995). Where freedom is given, liberties are taken. *Structure* 3, 535–540.
48. Kabsch, W. & Sander, C. (1983). Dictionary of protein secondary structure: pattern recognition of hydrogen bonding and geometrical features. *Biopolymers* 22, 2577–2637.
49. Kraulis, P.J. (1991). MOLSCRIPT: a program to produce both detailed and schematic plots of protein structures. *J. Appl. Cryst.* 24, 946–950.
50. Barton, G.J. (1993). ALSCRIPT, a tool to format multiple sequence alignments. *Protein Eng.* 6, 37–40.
51. Laskowski, R.A., MacArthur, M.W., Moss, D.S. & Thornton, J.M. (1993). PROCHECK: a program to check the stereochemical quality of protein structures. *J. Appl. Cryst.* 26, 283–291.